THE IMPACT OF FLUID PROPETIES AND FLOW CONDITIONS ON THE MEASUREMENT OF RELATIVE PERMEABILITY FOR CO_2-BRINE SYSTEM

Ben Niu[13], John Crawshaw[13], and Sam Krevor[23]
1. Department of Chemical Engineering, Imperial College, London
2. Department of Earth Science & Engineering, Imperial College, London
3. The Qatar Carbonates and Carbon Storage Research Center, Imperial College, London

This paper was prepared for presentation at the International Symposium of the Society of Core Analysts held in Avignon, France, 8-11 September, 2014

ABSTRACT
We present the results of a numerical study of the measurement of relative permeability for the CO_2-brine system by the steady state (SS) and JBN type method. A two-dimension model was used to conduct a sensitivity study on both methods, evaluating the impact of fluid properties, flow conditions and core geometry. The sensitivity of history matching method on pressure and production profiles has also been performed. The capillary end effect and gravity segregation proved to be the two dominant factors for maximising the saturation range and minimising the relative error of experimental results.

INTRODUCTION
Saline aquifers greater than 750 m in depth are considered important storage sites among the various geological formations, due to the large potential storage capacity (Global storage capacity of 400-10000Gt of CO_2 [1]) and available technology adapted from oil and gas industry [2].

Successful, industrial scale, injection of carbon dioxide into deep saline aquifers will be dependent on the ability to model the flow of the fluid. The effectiveness of the models is in turn dependent on high quality laboratory measurements of basic multiphase flow properties such as relative permeability at reservoir conditions. As the depth of most injection sites is greater than 750 meters [3], the experimental pressure and temperature of the measurements on CO_2-brine relative permeability is usually above the critical point of CO_2 (T_c=31^{o}C and P_c=7.38 MPa).

Compared with experiments on typical oil-brine systems, however, a unique defining characteristic of the CO_2-brine system is its combination of high viscosity ratio and low density ratio. During the drainage process (brine displaced by CO_2), the high viscosity ratio, on the one hand, can result in early breakthrough, indicating that a board range of saturation (therefore relative permeability) can be measured at the effluent [5]. On the other hand, this unfavourable mobility ratio can cause the time before a useful saturation range and end point is achieved to become impractical [5]. Although the density ratio tends to be more similar to oil/brine systems than gas/brine systems, the generally lower

density of CO_2 relative to brine can also lead to gravity segregation of the fluids in a high permeability sample and at low injection rate [6]. This can result in rate-dependent displacement efficiency, amplified by the high viscosity ratio and heterogeneity of the core sample [7]. Therefore, this combination of properties results in unique complications for experiments with CO_2 and brine and unique flow conditions must be used to achieve the combined goals of observations across a large saturation range and the avoidance of the error-inducing effects of heterogeneity, capillary forces and gravity segregation.

Several experimental studies of CO_2-brine flow system have been performed on different rocks, most of them on sandstone. However, it is difficult to compare those experimental results even with a single rock type, e.g., Berea sandstone, because they were conducted on core samples with different dimensions (Length: 5cm-15cm) across a wide range of temperature (20–75^{o}C) and pressure (3.5-20MPa), and with various brine composition (0-175g/l), [8]-[10] which results in different interfacial tension (IFT), viscosity and density ratios for the fluids. The relative permeability curves are determined by different techniques: both steady state method [9] and history matching technique [10]. Other than above factors, firing rock samples at high temperature to avoid the complication of mobile clay may make the sample more water-wet. However, this point is beyond the scope of our research.

Therefore, in this study, one and two-dimensional models have been created in a black oil reservoir simulator using as input characteristic relative permeability curves representative of typical Berea sandstone. We first compare results from steady state tests and unsteady states using JBN method. By comparing the simulated observables with the input properties, the impact of fluid properties and flow conditions on the measurement of relative permeability for the CO_2-brine system can be evaluated. Then, the sensitivity of history matching technique on different conditions has also been evaluated.

SIMULATION OF CORE FLOODING EXPERIMENTS

Model description: Multidimensional numerical models have been created with a characteristic relative permeability curve representing typical Berea sandstone. The steady state approach and unsteady state approach were simulated to obtain the apparent relative permeability. By comparing them, the impact of fluid properties and flow conditions on the measurement of relative permeability for CO_2-Brine system can be evaluated.

In our work, both 1-D and 2-D model were constructed to represent an axial slice from the middle of a Berea sandstone rock core with dimensions 3.8cm (1.5inches) in diameter and 30cm (12inches) in length. The 1-D homogeneous model was used for validation with an analytical solution and the 2-D model was the main tool for simulating CO_2-brine immiscible flow in the rock sample, and identifying an optimum set of experimental parameters for the successful design of flow experiments. Ultimately a group of dimensionless parameters were used to summarise the optimum parameter space in a general sense. Because the heterogeneity of rock is very case dependent and difficult to

include into dimensionless parameters, our 2-D model is homogeneous and we mainly focus on various flow properties and flow conditions, and different interpretation techniques.

The results from the base model were used to compare with those obtained under different conditions. The physical properties of the base model are described in Table 1. The simulated experimental conditions are typical for supercritical CO_2 sequestration and were based on the literature from existing experiments on Berea sandstone [8]-[10]. The density ρ, viscosity μ, and IFT σ of CO_2 and brine are calculated from well-established correlation models [11][12].

The Brooks-Corey model was used to describe the relative permeability of multiphase flow systems, as in Eqs. (1) and (2), where S is saturation, subscripts w, nw and r represent wetting phase, non-wetting phase and residual respectively. n_w and n_g are Corey exponents for water and CO_2. The characteristic permeability for base model is chosen to represent data from experiments on relative permeability in Berea sandstone [9][13], as shown in the Figure 4. The values of parameters are in Table 1.**Error! Reference source not found.Error! Reference source not found.**

$$k_{rw} = \left(\frac{S_w - S_{wr}}{1 - S_{wr}} \right)^{n_w} \quad (1) \qquad k_{rg} = \left(\frac{1 - S_w - S_{nwr}}{1 - S_{wr}} \right)^{n_g} \quad (2)$$

To model the drainage capillary pressure curves [14], the Brooks-Corey equation was used in our simulation, Eqs. (3) and (4).

$$P_c = P_e \left(S_* \right)^{-1/\lambda} \quad (3) \qquad S_* = \frac{S - S_{wr}}{1 - S_{wr}} \quad (4)$$

Where, P_e is the entry pressure for the invasion of CO_2 into the core sample, S_* is the normalized water saturation, and λ is the pore size distribution index. This equation was used to fit the data converted from mercury injection capillary pressure (MICP) on Berea sandstone by assuming it was strongly water wet [9]. The values of P_e and λ used in the base case were 2.67KPa and 0.67 respectively.

Simulation procedure and boundary conditions: The simulation tool used in this work was the adaptive implicit-explicit black oil simulator (IMEX®) from the computer modelling group (CMG). Carbon dioxide and brine are immiscible by default in the black oil simulator, which is consistent with the situation in SS and unsteady state (USS) experiments. In the SS experiment CO_2 and brine were injected into an initially 100% brine saturated core with increasing CO_2 ratios, from 5% to 100%. At each ratio, the criteria for steady state was that the variation of core average saturation and pressure drop was less than 0.05 between consecutive injected pore volumes [15].

Boundary slices were added to both inlet and outlet ends of the core, having the same dimension and properties as the rock slices [13]. Constant injection rate-controlled well and constant bottom hole pressure controlled wells were completed in the grid elements of the inlet and outlet boundary slices respectively. In addition, linear relative permeability was used for the inlet and outlet slices to allow full mobility for each phase. At the inlet boundary, CO_2 and brine were injected at a fraction of the total injection rate. The capillary pressure between two phases is set to zero at the inlet. At the outlet boundary, the capillary pressure between two phases is set to a constant equal to the entry capillary pressure P_e.

The relative permeability for the SS method can be calculated from the two-phase formulation of Darcy's law, Eq. (5), where *i* represents different phases.

$$k_{r,i} = \frac{q_i \mu_i L}{kA(P_{nw,inlet} - P_{w,outlet})} \quad (5)$$

The relative permeability for the USS can be calculated using the JBN method [16], Eqs. (6)-(9),

$$k_{rg,outlet} = f_{g,outlet} \frac{d\left[\frac{1}{\bar{Q}}\right]}{d\left[\frac{k\Delta P}{u_t u_g}\right]} \quad (6) \qquad k_{rw,outlet} = \frac{(1-f_{g,outlet})}{f_{g,outlet}} \cdot \frac{k_{rg,outlet}\mu_w}{\mu_g} \quad (7)$$

$$f_{g,outlet} = 1 - \frac{dS_{av,g}}{d\bar{Q}} \quad (8) \qquad S_{g,outlet} = S_{av,g} - \bar{Q}(1-f_{g,outlet}) \quad (9)$$

Where $\bar{Q}$ is the dimensionless total liquid production, the ratio between total liquid production and pore volume. Subscript *av* denotes average properties in the core. The calculation of pressure drop ΔP is the same as in SS method.

To evaluate the sensitivity of history matching technique in USS method, artificial errors and noises are added to the production and pressure profiles from Base case, and commercial software Sendra® is used to match the those profiles.

Dimensionless parameters: In order to evaluate the effect of fluid properties and the geometry of the core sample on the difference between characteristic relative permeability and apparent relative permeability, the dimensionless parameters [17], gravity number N_g, capillary number N_c and effective shape number R_l were used, Eqs. (10)-(12).

$$N_g = \frac{\Delta\rho g D k_h}{Lq\mu_o} \quad (10) \qquad N_c = \frac{P_c^* k_h}{Lq\mu_o} \quad (11) \qquad R_l = \left(\frac{L^2}{D^2}\right)\frac{k_v}{k_h} \quad (12)$$

Where, k_h and k_v are the permeability at horizontal and vertical direction respectively (equal in our simulation). P_c^* is the average capillary pressure of the medium,

$$P_c^* = \int_{S_{wr}}^{1} \frac{P_c(S_w)}{(1-S_{wr})} dS \quad (13)$$

Results and discussion: The results from the 1-D model matches well with the analytical solution without considering capillary pressure, as shown in Figure 2. With proper numerical control, the results are less sensitive to the number of elements. The model with capillary pressure agrees well with solution from Sendra®, as in Figure 3. Figure 4 shows the profiles from Base case. With increasing CO_2 ratio, the pressure drop is rising, and reaches maximum at the lowest total mobility, $M_t=k_w/\mu_w+k_g/\mu_g$.

In case PT1, the pressure and temperature are 11.3MPa and 117°C respectively, which keeps the IFT the same as in the base case, however, the viscosity ratio (μ_w/μ_{co2}) was changed from 19.6 to 11.9 for PT1. The pressure, 5.8MPa, and temperature, 86°C, in case PT2 changed the IFT from 37.4mN/m in the base case to 46.5mN/m, while holding the viscosity ratio constant. In Figure 5, the apparent relative permeability curves obtained by the SS method in the threes case agreed well with the characteristic relative permeability, except for the end point at residual water saturation. This discrepancy is mainly due to the capillary end effect, which leads to an increasing water saturation gradient towards the outlet of the cores and results in an erroneous average saturation at the highest fractional flows of CO_2. This influence is more pronounced on the relative permeability of non-wetting phase, CO_2. The results from the USS simulations were similar to those from SS methods, except the saturation range, which is due to the fact that the JBN method only works after breakthrough. Although the fraction of CO_2 in the flow is 99% before reaching the end point (100% CO_2), there was still a large gap on the relative permeability curve.

The effect of core length, diameter, permeability, capillary pressure on SS method and JBN type method has also been evaluated. The results are similar to the above observation at different pressure and temperature conditions, and not shown in this paper due to limited space.

In the case with high injection rate, a lower end point can be obtained; however, there is no improvement with other fractional flows, as shown in Figure 6. The apparent relative permeability curve starts to be influenced by gravity segregation at low injection rate, especially with the JBN methods. Although both gravity segregation and capillary pressure can induce early breakthrough, the former result in larger errors in CO_2 relative

permeability for CO_2-brine system. In real experiment, the local heterogeneity of capillary pressure can be more important than gravity segregation. However, this is out of our discussion here.

The observed relative permeability from various conditions was compared with the characteristic relative permeability in terms of the observable saturation range and the relative error (ratio between the maximum absolute error and simulated results), as shown in Figure 7. Based on the dimensionless parameters in Eqs. (10)-(12), these two parameters can be catalogued, as in Figure 8 and Figure 9. For the same effective shape factor R_l, for example, a large saturation range and smaller error can be obtained with decreasing capillary and gravity numbers. This observation suggests a simple approach for using those parameters to design CO_2-brine experiments with highly accurate results for relative permeability.

It is important to note that SS method and JBN method are not influenced significantly by various reservoir conditions in simulation for CO_2-brine system. Because variation of fluid properties of CO_2 and brine are not large enough to make impact on relative permeability measurement. For instance, recent experimental results have confirmed that the variation of IFT from 20-56mN/m (CO_2 from supercritical to gas phase) has no influence on relative permeability measurement [19]. The effect of interfacial tension on relative permeability starts to work when IFT smaller than 1mN/m for oil/water system [19]. It is reasonable to assume CO_2-brine system has threshold value at similar magnitude. Therefore, among the conditions for supercritical CO_2 injection, the relative permeability measurement should be less sensitive to the change of IFT.

History match is industry standard approach [8] and has better performance than JBN method. Because SS method and JBN method matched perfectly the input curve due to above reasons, there is no reason to repeat previous steps. We specifically evaluate the sensitivity of history match to, e.g. perturbations in the pressure or production signal.

The history matching results on Base case are shown in Figure 10 and Figure 11. The production and pressure profiles have been matched well. The apparent relative permeability from history matching is almost the same as characteristic relative permeability. Moreover, the low viscosity ratio between CO_2 and brine make the displacement in low efficiency. In the base case on SS method, we deliberately flash the core for 3300PVI (pore volume injected), the end point water saturation in Figure 11 is still affected by the capillary end effect.

To examine the sensitivity of history matching technique, the pressure data are allowed to change up to ±14% on the original profiles to simulate the scenario that pressure transducers are not well calibrated or have erroneous recording. The history matching results on pressure sensitivity are shown in Figure 12 and Figure 14. In CO_2-brine system, the gas phase (non-wetting) is affected more seriously by the error on pressure.

With decreasing pressure difference, irreducible water saturation is increasing and gas relative permeability is decreasing.

To simulate the case with erroneous production profile, which is usually encountered in the lab due to dead volume and leakage in the experimental setup, the water production data are allowed to change up to ±10% on the original profiles. Figure 13 and Figure 15 show the history matching results on production sensitivity. Relative permeability curves for both CO_2 and brine have been affected by introduced errors on water production, and the former is much vulnerable to these changes. The underestimation of water production tends to shift the relative permeability curve to left side (direction of increasing water saturation) of characteristic relative permeability curve.

CONCLUSION

We have used a detailed simulation model to evaluate the sensitivity of the steady state method and the unsteady state method for the measurement of relative permeability for the CO_2-brine system at various conditions. The results suggest that capillary end effect is the major error source in the SS method, particularly at the end point. However, at low injection rates up to 0.4cc/min, gravity segregation becomes the dominant factor. The saturation range and relative error were analysed using a group of dimensionless parameters, which can be used for future experiment design. The sensitivity of history matching suggests that gas relative permeability is more sensitive to the error on pressure and production profiles.

ACKNOWLEDGEMENTS

We gratefully acknowledge financial support from Qatar Petroleum, Shell and Qatar Science and Technology Park.

REFERENCES

1. F.M. Orr Jr., Storage of carbon dioxide in geological formation, Journal of Petroleum Technology, 56(9): 90 – 97, 2004.
2. S.M. Benson and F. M. Orr Jr., Carbon dioxide capture and storage, MRS Bulletin, 33(4): 303-305, 2008.
3. J.M. Nordbotten, M.A. Celia and S. Bachu, Injection and storage of CO_2 in deep saline aquifers: analytical solution for CO_2 plume evolution during injection, Transport in Porous Media, 58(3): 339-360, 2005.
4. D.J. O'Meara Jr. and W.O. Lease, Multiphase relative permeability measurements using an automated centrifuge, Paper SPE 12128 presented at SPE Annual Technical Conference and Exhibition, San Francisco, California, 5-8 October, 1983.
5. S. Benson, R. Pini, C. Reynolds and S. Krevor, Relative permeability analysis to describe multi-phase flow in CO_2 storage reservoirs, 07 August, 2013.
6. V. Nilsen, Y. Guo and F. Hovland, Gravity effect under steady-state and unsteady state core flooding and criteria to avoid it. Presented at the International Symposium of the Society of Core Analysts held in San Antonio, TX, USA, 1991.

7. M.A. Crotti and J.A. Rosbaco, Relative permeability curves: the influence of flow direction and Heterogeneities, Paper SPE 39657 presented at the SPE/DOE Improved Oil Recovery Symposium, Tulsa, Oklahoma, 19-22 April, 1998.
8. M. Akbarabadi, and M. Piri, Relative Permeability hysteresis and Capillary Trapping Characteristics of Supercritical CO_2-brine Systems: An Experimental Study at Reservoir Conditions, Advances in Water Resources 52: 190-206, 2013.
9. S. Krevor, R. Pini, L. Zuo and S. Benson, Relative permeability and trapping of CO_2 and Water in Sandstone Rocks at Reservoir Conditions, Water Resources Research, 48(2): W02532, 2012.
10. S. Berg, S. Oedai and H. Ott, Displacement and mass transfer between saturated - and unsaturated CO_2-brine systems in sandstone, International Journal of Greenhouse Gas Control, 12: 478-492, January 2013.
11. J.M. Lombard, F. Martina, P. Egermann, C. Chalbaud, M. Robin and H. Bertin, Interfacial tension measurement and wettability evaluation for geological CO_2 storage. Advances in Water Resources, 32(1):98-109, January 2009.
12. J. Kestin, H.E. Khalifa and R.J. Correia, Tables of the dynamic and kinematic viscosity of aqueous NaCl solutions in the temperature range 20-150^{o}C and the pressure range 0.1-35MPa, Journal of physical and chemical reference data, 10:71-87, 1981.
13. C.W. Kuo, J.C. Perrin and S. Benson, Effect of gravity, flow rate, and small scale heterogeneity on multiphase flow of CO_2 and brine, Paper SPE 132607 presented at SPE Western Regional Meeting, Anaheim, California, USA, 27-29 May, 2010.
14. K.W. Li, Theoretical development of the brooks-corey capillary pressure model from fractal modeling of porous media, Paper SPE 89429 presented at the SPE/DOE Symposium on Improved Oil Recovery, Tulsa, Oklahoma, 17-21 April, 2004.
15. M.H. Krause, Modelling and investigation of the influence of capillary heterogeneity on relative permeability, Paper SPE 160909 presented at the SPE Annual Technical Conference and Exhibition, San Antonio, Texas, USA, 8-10 October, 2012.
16. D.P. Bossler, E.F. Johnson and V.O. Naumann, Calculation of relative permeability from displacement experiments. Petroleum Transactions, 216: 370-372, 1959.
17. D. Zhou, F.J. Fayers and F.M. Orr Jr., Scaling of multiphase flow in simple heterogeneous porous media, Paper SPE 27833 presented at the SPE/DOE ninth Symposium on Improved Oil Recovery held in Tulsa, Oklahoma, USA, 17-20 April, 1994.
18. R. Pini, and S. Benson, Simultaneous determination of capillary pressure and relative permeability curves from core-flooding experiments with various fluid pairs. Water Resource Research, 49: 3516-3530, 2013.
19. S. Kumar, S.J. Torabzadeh, and L.L. Handy, Relative permeability functions for high- and low- tension systems at elevated temperatures, Paper SPE 13670 presented at the SPE 1985 California Regional Meeting, Bakersfield, California, March 27-29, 1985.

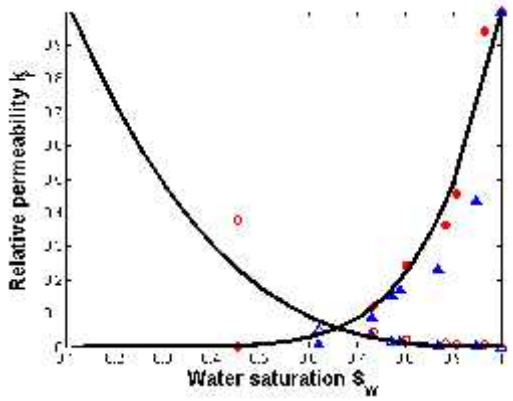

Figure 1 Characteristic relative permeability used in Base model (Black line). Drainage CO2 (open) and brine (solid) data from Krevor et al. 2012 (red) [9] and Kuo et al. 2010 (blue) [13].

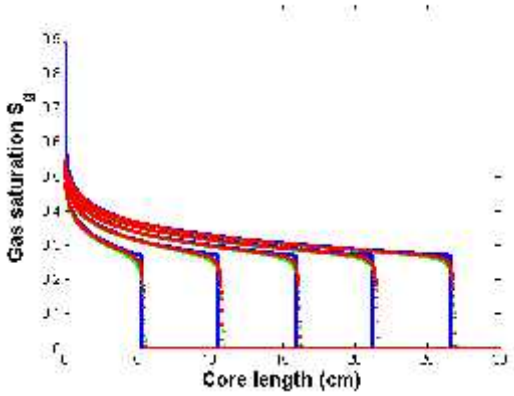

Figure 2 Comparison between analytical solution and CMG solution without capillary pressure: Blue line: the analytical solution. Green triangle: numerical solution with 500grids. Red square: numerical solution with 1500 grids.

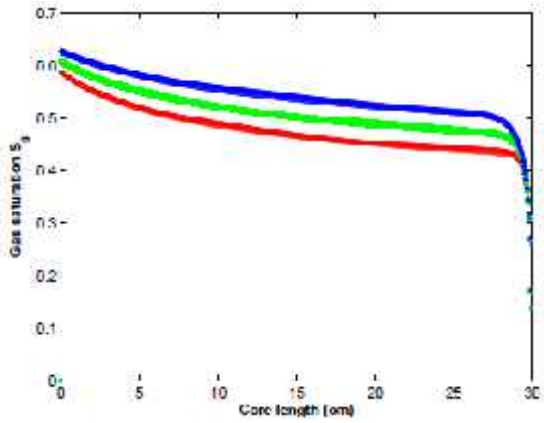

Figure 3 Comparison between solution from CMG (Open) and Sendra® (solid) with considering capillary pressure: Red: 30mins, Green: 60mins, Blue: 120mins.

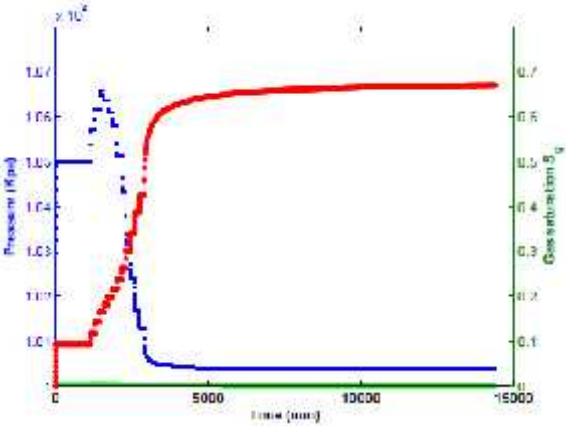

Figure 4 Average saturation and pressure profiles from Base case. Blue square: inlet pressure. Green triangle: outlet pressure. Red circle: CO_2 saturation

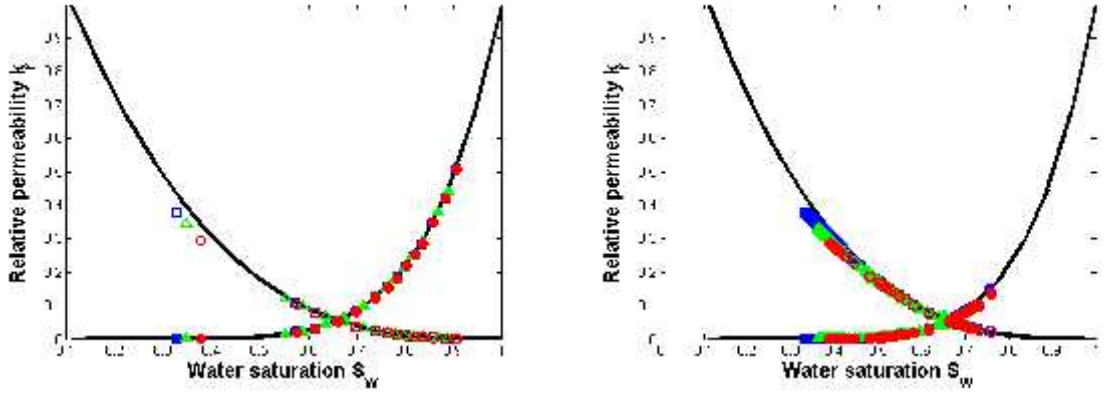

Figure 5 Comparison between apparent relative permeability by SS method (Left) and JBN analysed method (Right) (krg: open, krw: solid): Blue square: base case, Green triangle: PT1. Red circle: PT2.

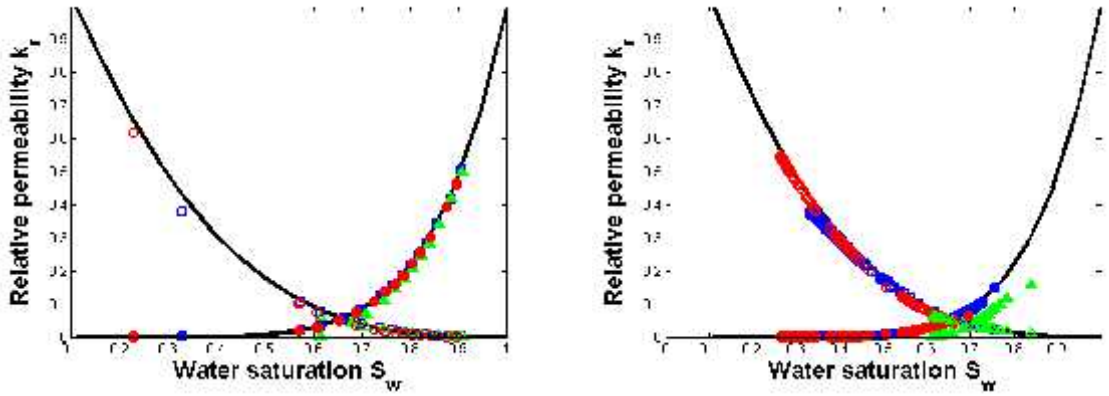

Figure 6 Comparison between apparent relative permeability by SS method (Left) and JBN analysed method (Right) (krg: open, krw: solid): Blue square: base case, Green triangle: 0.4cc/min. Red circle: 200cc/min.

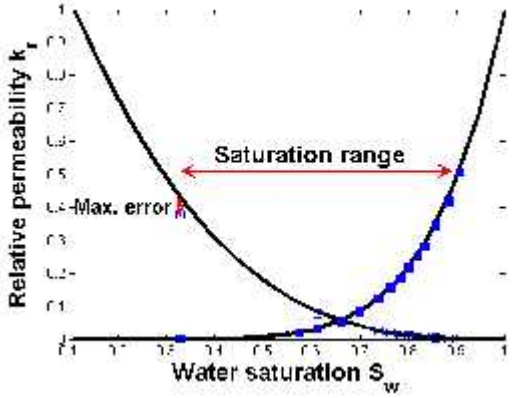

Figure 7 Definition of saturation range and Maximum error

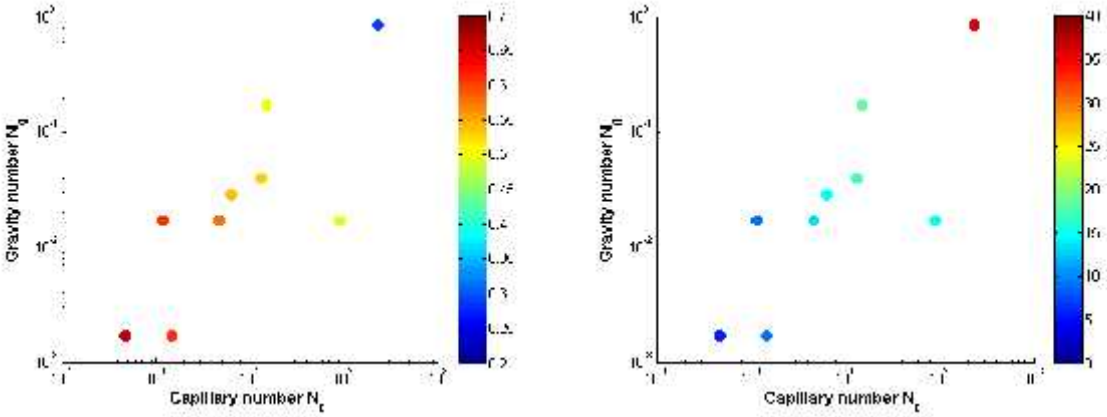

Figure 8 Distribution of saturation range (left) and maximum error range (%) in the dimensionless space at R_l =62

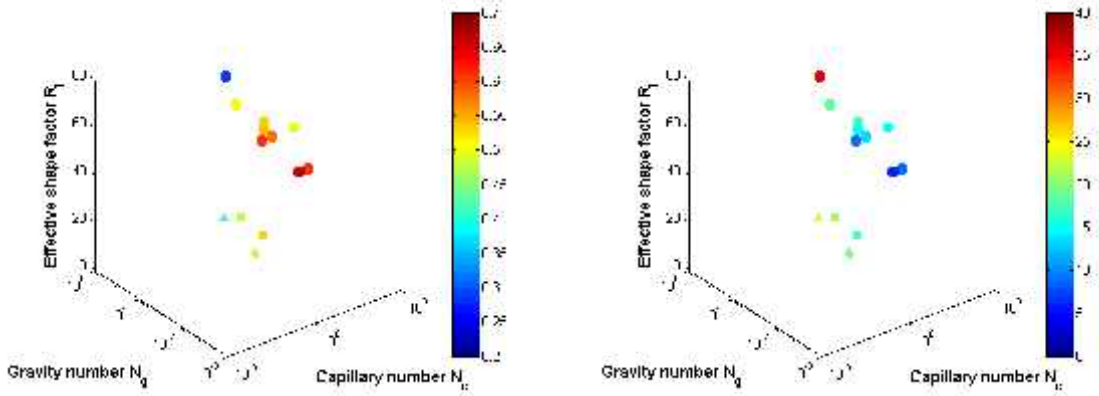

Figure 9 Distribution of saturation range (left) and maximum error range (%) in the dimensionless space. R_l: Circle 62, Square 15.5, Triangle 6.9, Diamond 3.9.

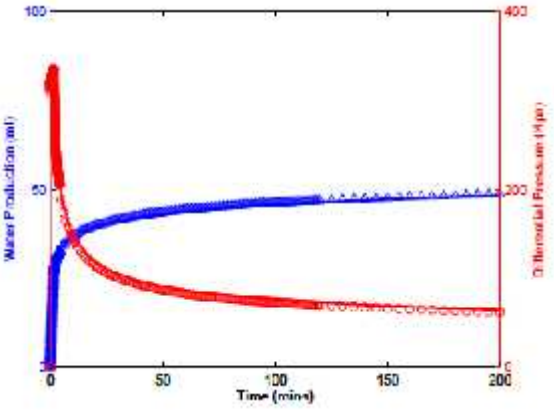

Figure 10 History matching on Base case. Blue Triangle: water production. Red Circle: Differential pressure. Line: history matching results.

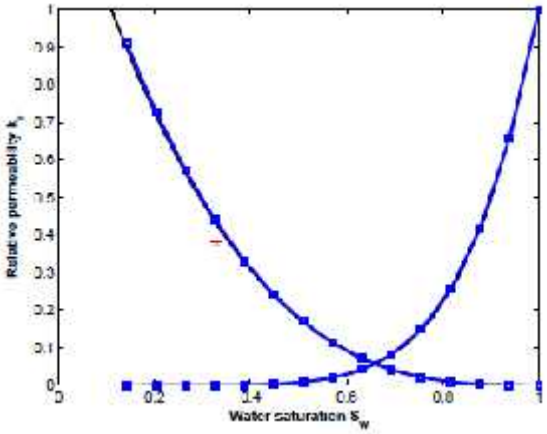

Figure 11 History matching on Base case. Black Line: characteristic permeability, Blue square with line: history matching result. Red star: end point value.

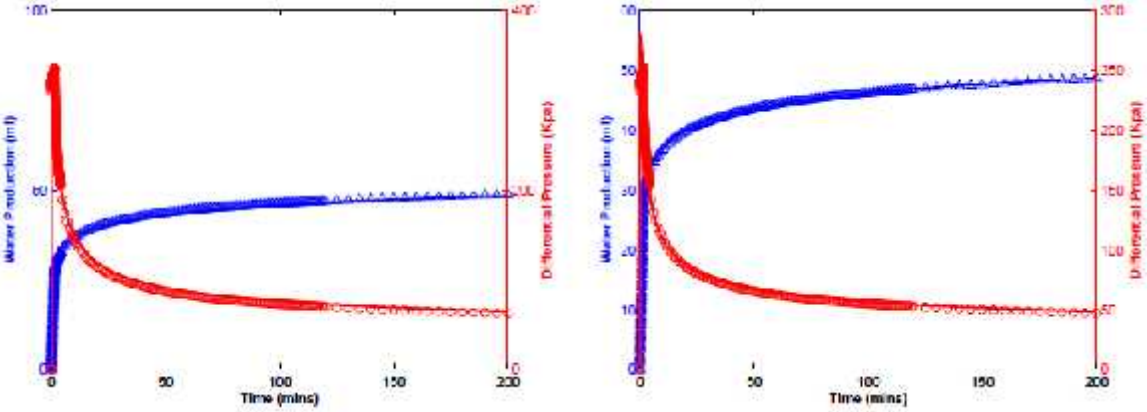

Figure 12 Production sensitivity of history matching – profiles, 14% higher differential pressure (Left) and 14% lower differential pressure (Right). Blue triangle: water production from, Red circle: differential pressure. Lines: History matching results.

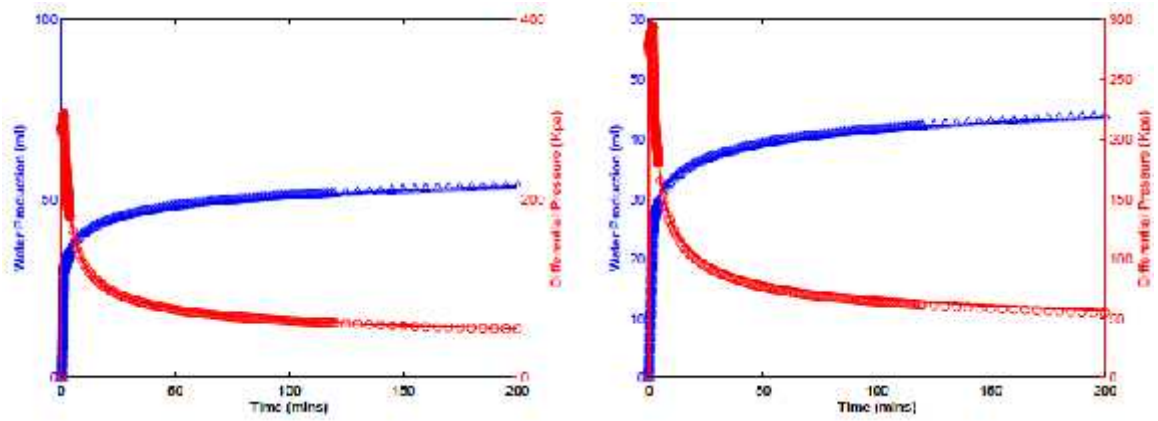

Figure 13 Production sensitivity of history matching – profiles, 10% higher water production (Left) and 10% lower water production (Right). Blue triangle: water production, Red circle: differential pressure from Base case. Lines: History matching results.

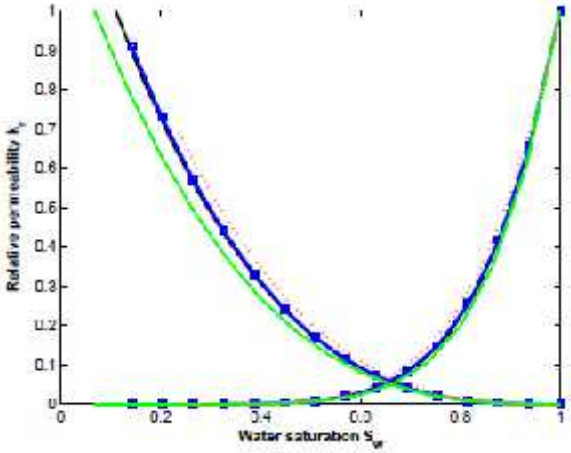

Figure 14 Pressure sensitivity of history matching – relative permeability. Black line: Characteristic relative permeability, Blue square with line: history matching result. Green line: 14% higher differential pressure, Red dot line: 14% lower differential pressure.

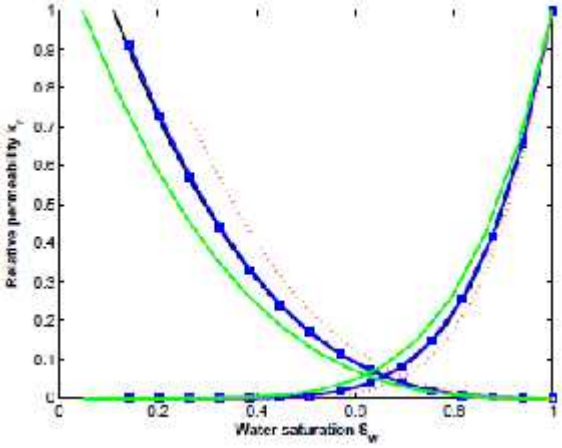

Figure 15 Pressure sensitivity of history matching – relative permeability. Black line: Characteristic relative permeability, Blue square with line: history matching result. Green line: 10% higher water production, Red dot line: 10% lower water production.

Table 1 Core properties and experimental conditions for base model

Ø(%)	25	L(cm)	30	Swr	0.11
K(mD)	200	T(^{o}C)	50	Snwr	0
D(cm)	3.8	P(MPa)	10	λ	0.67
ρw(kg/m3)	1.03	NacCl(mol/kg)	1	nw	6
ρco2(kg/m3)	0.3963	μw(CP)	0.031	ng	3
σ(mN/m)	37.36	μco2(CP)	0.6106	Q(cc/min)	20